Computers and Geotechnics 164 (2023) 105788

Contents lists available at ScienceDirect

Computers and Geotechnics

journal homepage: www.elsevier.com/locate/compgeo

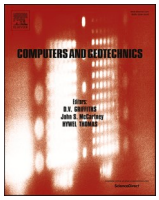

A finite layer analysis method proposed for energy pile modeling under coupled thermo-mechanical loads

Chenfeng Zong [a], Gang Jiang [a,*], Dong Shao [b,*], Xudong Wang [a], Wenbin Hu [a]

[a] College of Transportation Science & Engineering, Nanjing Tech University, Nanjing, 210009, China
[b] Key Laboratory for Mechanics in Fluid Solid Coupling Systems, Institute of Mechanics, Chinese Academy of Sciences, Beijing, 100190, China

ARTICLE INFO

Keywords:
Energy piles
Thermo-mechanical load
Finite layer analysis method (FLM)
Coupled thermo-mechanical analysis

ABSTRACT

This study proposes a new hybrid analytical and numerical approach to analyze energy piles by coupling thermal and mechanical loads. Conceived through the finite unit method, the Finite Layer Analysis Method (FLM) boasts promising results when applied to energy piles in soil, which is typically layered or multilayer mediums. This methodology effectively reduces a complex, three-dimensional geotechnical problem to two dimensions, yielding marked improvements in computational efficiency. The FLM for energy pile consists of temperature field calculation and thermo-mechanical coupling calculation, for which the theory and derivation are carefully introduced and elaborated. To validate the accuracy and robustness of the newly proposed FLM method, both the temperature field calculation and the thermo-mechanical coupling calculation are verified meticulously with the finite-length heat source analysis theory, together with the Finite Element results. The validations are also performed against a variety of field trial data including those from London and Lausanne tests.

1. Introduction

As the greenhouse gas emissions have resulted in significant environmental problems (Bölük and Mert, 2014; Sugiawan and Managi, 2019), many governments begin to strategically encourage the use of renewable energies (Sørensen, 2008; Abas et al., 2015). As the geothermal energy presents an attractive renewable energy source, the integration of shallow geothermal energy systems, also known as SGES, into conventional drilled shaft foundations has become an appealing option for the energy alternative in a number of countries for the domain of civil engineering and construction industry (de Moel et al., 2010). This engineering practice is also known as energy pile technique. Energy piles can use the ground as a heat source in winter and a heat sink in summer for the thermal control of a building since the ground temperature remains constant and stable regardless of how the outside air temperature changes with the seasons. It has been estimated that the technique may represent up to 70% reduction in fossil fuels for the heating and cooling of the buildings (Brandl, 2006; Murphy et al., 2013).

When the concept of energy piles was initially conceived, the primary concentration was placed on how well they conveyed heat, and a number of field experiments were carried out to investigate how beneficial they were from the point of view of heat transmission (Brandl, 2006; Bourne-Webb et al., 2009; Kramer, 2013). Among the in situ experiences of the energy pile responses to thermal and mechanical loads, some results remarked that the variation of temperature induced significant change in mobilized shaft friction and axial load distribution in the energy piles at the pile-soil interface and the remarkable changes were revealed to depend on the axial fixity of the head and the toe of the energy piles (Armaleh and Desai, 1987; Bourne-Webb et al.,2009; Laloui et al., 2006; Amatya et al.,2012). Although the pile load test in field presents a reliable method for observing and determining the thermal–mechanical behaviors of energy pile, it is manifestly both time-consuming and costly and requires numerical modeling approaches as more efficient alternatives. The findings of field tests may also be furthermore synthesized into the form of numerical model to provide quantitative predictions of energy pile behavior in different settings.

Knellwolf et al. (2011) conducted one of the first numerical studies of energy pile to consider thermo-mechanical load transfer analysis on the basis of the conventional load transfer analysis method for mechanical loading. The energy pile was divided into a number of elastic foundation elements attached to the soil with the connection assumed to be elastic perfectly-plastic springs. Comparably, Plaseied (2012) induced nonlinear springs into the numerical model with hyperbolic curves representing the mobilized side shear and end bearing resistance. The

* Corresponding authors.
E-mail addresses: g.jiang@njtech.edu.cn (G. Jiang), dshao@njtech.edu.cn (D. Shao).

https://doi.org/10.1016/j.compgeo.2023.105788
Received 31 March 2023; Received in revised form 17 July 2023; Accepted 7 September 2023
Available online 21 September 2023

effect of radial expansion of the energy pile was also taken into account. In applying an assumed shape of the mobilized side shear resistance and end-bearing resistance curves with knowledge of the ultimate side shear and end-bearing capacities, the load transfer approach provides the possibility of accounting for the complex interaction between soils and foundations during mechanical and thermal loading via theoretical curves at the interface and can estimate the distribution of axial stress, strain, and displacement with depth (Suryatriyastuti et al., 2014). However, it requires the exact location of the null-point (which the algorithm often fails to capture due to the finitely small size of the elements in coordination with the convergence threshold) along the energy pile to avoid potentially inaccurate results.

In another scope, since numerous applications of finite element (FE) studies have been carried out with the goal of predicting the behavior of pile foundations subjected to mechanical forces (Castelli and Maugeri 2002; Leung et al. 2010; Said et al. 2009), they have also been employed in the prediction and analysis of behaviors of energy pile in heating and cooling conditions including the heat transfer capacity with temperature variations, the axial displacements and the distributions of strain and stress (Laloui et al. 2006; Ouyang et al. 2011; Wang et al. 2012, 2015; Donna and Laloui, 2015). Although FE analyses can show good correlations with field data for the normal pile foundations as well as for the energy pile foundations, they are generally challenging to be performed for energy pile design because of the difficulty of determining the large number of input factors or parameters required in simulating the behavior of the soil, the pile and also the interface between them, especially when nonlinear characteristics are taken into account.

As an alternative either to the sometimes oversimplified load transfer method or to the complicated time-consuming finite element method, the finite layer method (FLM) can be readily applied to the analysis of structural responses of energy piles in solving both the temperature field and the mechanical one. The finite layer method can be regarded as a semi-analytical FEM method which discretizes the computational domain in one dimension (the depth direction for the pile analysis) in formulating the solution with Fourier series in the two other horizontal dimensions. The finite layer method began to take shape from its embryo version named as finite strip method for two-dimensional elastic analysis (YK Cheung, 1976). With the series-form approximation in place of discretization in one of the two directions, the finite strip method increases the computational efficiency without sacrificing the accuracy (sometimes even found to be superior to the comparable finite element method). The finite strip method was then extended to heat conduction problem (Chakrabarti, 1980) with a comparability to the temperature field analysis of energy pile studied in this work. When extended to three-dimensional problems, the finite strip method becomes the finite layer method (FLM) which is particularly suitable for the analysis of multilayered media and structures. Since the fundamental theory and application were proposed in 1979, the FLM has been utilized in the study of horizontally stratified elastic foundations. Subsequently, the method was refined for the investigation of heterogeneous soils with a linear distribution of the modulus with depth (Booker and Small, 1982). A finite layer flexibility matrix was developed to alleviate the issues encountered when using the usual finite layer stiffness method to incompressible solids (Booker and Small, 1984). In the years that followed, the FLM was applied in the assessments of three-dimensional consolidation of layered transversely isotropic soils (Mei and Zai, 2006) and the soil-pile interactions (Wang et al., 1994, 1996). The groundwater flow and the soil consolidation and surface deformation involving water extraction were also studied using this method (Booker and Small, 1982, 1986; Small and Booker, 1986; Smith et al., 1992; Wang et al., 2009).

As a whole, the FLM presents a simplified version of FE analysis method but with a good effectiveness when applied to stratified or multilayered media like the soil. Compared to the more analytical load transfer methods typically used in geotechnical studies, the Finite Layer Method (FLM) that accommodates soil non-homogeneity operates differently. The FLM is grounded in the analysis of soil within a semi-infinite space, deriving the soil deformation within this semi-infinite space, and subsequently incorporating these findings into the analysis of pile-soil interaction. Notably, this approach does not necessitate any a priori assumptions regarding the interaction curve at the pile-soil interface. For the calculation of the thermo-mechanical responses of energy pile, the FLM may have the capacity of determining the temperature field and coupling it with the mechanical loads. To the best of our knowledge, the FLM has not yet been formulated and applied for the modeling of energy pile.

In the following sections of this paper, the formulations of the FLM for energy pile modeling under coupled thermos-mechanical loads are firstly introduced with a brief description of the basic theory. Subsequently, the model is validated against the analytical, numerical and field observation data from the literature. The conclusions are drawn in the last section.

2. Methodology

2.1. Calculation of Soil Temperature Field

Assume a finite area with homogeneous soil and a buried pipe with constant heat flow at the center of the calculation area (shown in Fig. 1), according to Fourier's law and the law of conservation of energy, the differential equation of heat conduction in the right-angle coordinate system can be expressed as Eq. (1).

$$\lambda_x\frac{\partial^2 T}{\partial x^2}+\lambda_y\frac{\partial^2 T}{\partial x^2}+\lambda_z\frac{\partial^2 T}{\partial x^2}+q(x,y,z,t)=\rho c\frac{\partial T}{\partial t} \tag{1}$$

with the initial moment stratum temperature (T_0) is uniformly distributed. Let $\tau = T\text{-}T_0$, so the heat conduction equation corresponding to the initial condition can be expressed as

$$\tau(x,y,z,0)=0\ 0\leqslant x\leqslant a,\ 0\leqslant y\leqslant b,\ 0\leqslant z\leqslant c \tag{2}$$

With a constant temperature at the boundaries

$$\begin{cases}\tau(0,y,z,t)=\tau(a,y,z,t)=0\\ \tau(x,0,z,t)=\tau(x,b,z,t)=0\end{cases} \tag{3}$$

In introducing a differential operator $L(T)=\lambda_x\frac{\partial^2 T}{\partial x^2}+\lambda_y\frac{\partial^2 T}{\partial x^2}+\lambda_z\frac{\partial^2 T}{\partial x^2}-\rho c\frac{\partial T}{\partial t}$ and taking w as the trial function, the Galerkin equation of Eq. (1) can be transformed into Eq. (4).

$$\iiint_D (L(T)+q(x,y,t))\cdot w\ \mathrm{dxdydz}\ =\ 0 \tag{4}$$

With the laminar characteristics of the underground layers, the finite layer method (FLM) in the × and y planes may be represented by a two-dimensional analytic function, whereas a linear function is discretized in the z direction. The semi-analytic nature of FLM requires the creation of trial functions in the *xy* plane which satisfy the boundary conditions. For the temperature calculation, the trial function is formulated as

$$\tilde{\tau}(x,y,z,t)=\sum_{j=1}^{L+1}\sum_{m=1}^{M}\sum_{n=1}^{N}\Phi_{mnj}(t)A_{mn}(x,y)N_j(z) \tag{5}$$

with $\Phi_{mnj}(t)$ indicating the coefficient to be found, M and N the number of terms of the series and L representing the total number of finite layers layer elements. As a standard linear interpolation shape function, $N_j(z)$ can be expressed as

$$N_j(z)=\begin{cases}(z-z_{j-1})/(z_j-z_{j-1})(z_{j-1}\leqslant z\leqslant z_j)\\ (z-z_{j+1})/(z_j-z_{j+1})(z_j\leqslant z\leqslant z_{j+1})\\ 0(z\leqslant z_{j-1}orz\geqslant z_{j+1})\end{cases} \tag{6}$$

$A_{mn}(x, y)$ is taken from a sequence of complete orthogonal functions that should make the temperature trial function satisfy the constant temperature boundary condition, which is given as

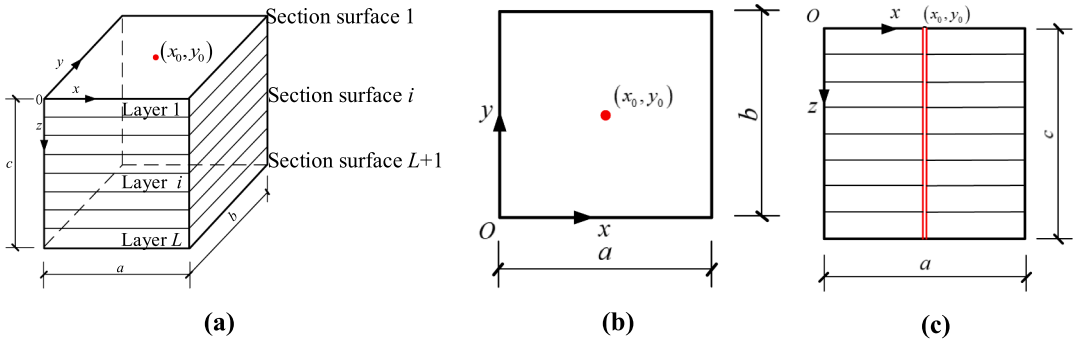

Fig. 1. Finite Layer Model (a) Finite layer physical model diagram (b) Top view of finite layer physical model (c) Sectional view of finite layer physical model.

$$A_{mn}(x,y) = \sin k_m x \cdot \sin k_n y \tag{7}$$

where $k_m = m\pi/a$, $k_n = n\pi/b$ with a and b the dimensions of the computational domain. Bring Eq. (5) into Eq. (4), and according to the orthogonality of the Fourier series, we can get the finite layer matrix representation of the mnth term of the layer element L with (8)

$$[R]^e_{mn}\{\Phi\}^e_{mn} + [F]^e_{mn}\frac{\mathrm{d}}{\mathrm{d}t}\{\Phi\}^e_{mn} + \{Q\}^e_{mn} = 0 \tag{8}$$

where $[R]^e_{mn}$ is the layer element heat transfer matrix, $[F]^e_{mn}$ is the layer element specific heat matrix, $\{Q\}^e_{mn}$ is the layer element heat vector and $\{\Phi\}^e_{mn}$ is the layer element coefficient vector to be determined. Eq. (8) can be further expanded to obtain the matrix coefficient expression for the finite layer equation.

$$\begin{bmatrix} r^e_{l,l} & r^e_{l,l+1} \\ r^e_{l+1,l} & r^e_{l+1,l+1} \end{bmatrix}_{mn} \begin{Bmatrix} \phi^e_l \\ \phi^e_{l+1} \end{Bmatrix}_{mn} + \begin{bmatrix} f^e_{l,l} & f^e_{l,l+1} \\ f^e_{l+1,l} & f^e_{l+1,l+1} \end{bmatrix}_{mn} \frac{\mathrm{d}}{\mathrm{d}t}\begin{Bmatrix} \phi^e_l \\ \phi^e_{l+1} \end{Bmatrix}_{mn} + \begin{Bmatrix} q^e_l \\ q^e_{l+1} \end{Bmatrix}_{mn} = 0 \tag{9}$$

where $r^e_{l,l}$ is the layer element heat transfer matrix coefficient, $f^e_{l,l}$ is the layer element specific heat matrix coefficient, q^e_l is the layer element coefficient vector coefficient and ϕ_l is the layer element coefficient to be determined. The expressions for the layer element heat transfer matrix coefficient (r_{mnij}) and the layer element specific heat matrix coefficient (f_{mnij}) are

$$r^e_{mnij} = \begin{cases} -ab/4\left\{\left[(\lambda_x)_l k_m^2 + (\lambda_y)_l k_n^2\right]\frac{c_l}{3} + \frac{(\lambda_z)_l}{c_l}\right\} & i = j \\ -ab/4\left\{\left[(\lambda_x)_l k_m^2 + (\lambda_y)_l k_n^2\right]\frac{c_l}{6} - \frac{(\lambda_z)_l}{c_l}\right\} & i \neq j \end{cases} \quad f^e_{mnij}$$
$$= \begin{cases} -\dfrac{abc_l\rho c}{12} & i = j \\ -\dfrac{abc_l\rho c}{24} & i \neq j \end{cases} \tag{10}$$

For modeling the energy pile, a constant heat flow (q) is located at the center of the computational domain. With the total heat exchange (Q_{total}) during energy pile operation and the pile length H, the heat exchange per unit pile length ($\overline{Q}(x_0,y_0)$) can be expressed as

$$\overline{Q}(x_0,y_0) = \frac{Q_{\text{total}}}{H} \tag{11}$$

and by applying the Dirac function, the heat flow vector coefficients of the layer elements can be obtained as

$$q^e_{mnij} = \int_{z_l}^{z_{l+1}} N_j \int_0^a \int_0^b \overline{Q}(x_0,y_0)\delta(x-x_0,y-y_0)A_{mn}\mathrm{d}x\mathrm{d}y\mathrm{d}z = \frac{c_l}{2}\cdot\overline{Q}(x_0,y_0)\cdot\sin(k_m x_0)\sin(k_n y_0) \tag{12}$$

The overall finite layer equation can be assembled according to Eq. (8).

$$[R]_{mn}\{\Phi\}_{mn} + [F]_{mn}\frac{\mathrm{d}}{\mathrm{d}t}\{\Phi\}_{mn} + \{Q\}_{mn} = 0 \tag{13}$$

Where $[R]_{mn}$ is the heat transfer matrix, $[F]_{mn}$ is the specific heat matrix, $\{Q\}_{mn}$ is the element heat vector and $\{\Phi\}_{mn}$ is the coefficient vector to be determined. The finite layer heat transfer matrix, specific heat matrix and heat flow vector of the unsteady thermal conductivity of the stratum in the right-angle coordinate system are assembled by superimposing the respective layer element matrices.

As the above-mentioned formulations present an unsteady thermal conductivity problem, the temperature can be discretized using finite difference scheme as

$$\frac{\mathrm{d}\{\Phi\}_{mn}}{\mathrm{d}t} = \frac{\{\Phi\}^{k+1}_{mn} - \{\Phi\}^{k}_{mn}}{\Delta t} \tag{14}$$

and a weighted average can be used to express it as

$$\{\Phi\}^{k+\theta}_{mn} = \theta\{\Phi\}^{k+1}_{mn} + (1-\theta)\{\Phi\}^{k}_{mn} \tag{15}$$

with $\{\Phi\}^{k}_{mn}$ and $\{\Phi\}^{k+1}_{mn}$ indicating the value of the corresponding coefficient for moments k and $k+1$, respectively. θ is a weighting factor and takes values between 0 and 1.

In combining Eq. (14) and Eq. (15) and bringing them into Eq. (13), the finite layer equation can be written as

$$\theta[R]_{mn} + \frac{1}{\Delta t}[F]_{mn}\{\Phi\}^{k+1}_{mn} = \left(\frac{1}{\Delta t}[F]_{mn} - (1-\theta)[R]_{mn}\right)\{\Phi\}^{k}_{mn} - \{Q\}^{k}_{mn} \tag{16}$$

According to the finite layer analysis method of energy pile in stratified strata, the corresponding calculation program is prepared, which can simulate the temperature change at any point in the stratum at any moment under different operation modes of energy pile. The diagram of the stratum temperature field program is shown in Fig. 2.

2.2. Calculation of Mechanics Field

Fig. 3(a) illustrates the physical model for the mechanics field calculation with FLM. The lateral boundaries of the computational domain can be seen as the roller boundary while the boundary condition at the bottom can be chosen rigidly rough or rigidly smooth as needed (shown in Fig. 3(b)). A typical layer element is displayed in Fig. 3(c).

The computational domain with dimensions $a \times b \times c$ is chosen to represent the half-space physical model and is divided into N layers in the vertical direction with five elastic constants applicable to each layer. The elasticity matrix can be expressed as

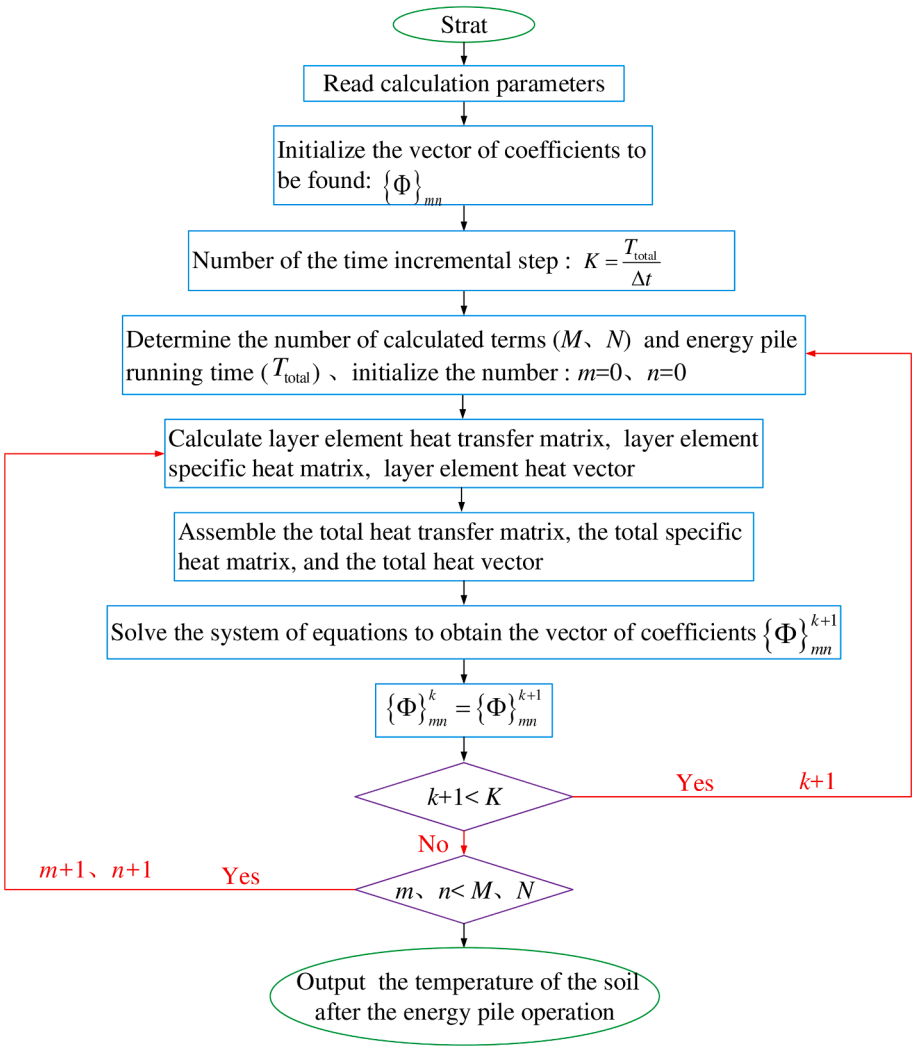

Fig. 2. Flow chart of the calculation procedure of the temperature field.

$$[D]=\begin{bmatrix} d_1 & d_2 & d_3 & 0 & 0 & 0 \\ d_2 & d_1 & d_3 & 0 & 0 & 0 \\ d_3 & d_3 & d_4 & 0 & 0 & 0 \\ 0 & 0 & 0 & d_5 & 0 & 0 \\ 0 & 0 & 0 & 0 & d_6 & 0 \\ 0 & 0 & 0 & 0 & 0 & d_6 \end{bmatrix} \tag{17}$$

$$d_1=\lambda n\left(1-n\mu_2^2\right)d_2=\lambda n\left(\mu_1+n\mu_2^2\right)d_3=\lambda n\mu_2(1+\mu_1)d_4=\lambda\left(1-\mu_1^2\right)$$

$$d_5=\frac{E_1}{2(1+\mu_1)}d_6=G_2\lambda=\frac{E_2}{(1+\mu_1)(1-\mu_1-2n\mu_2^2)}n=\frac{E_1}{E_2}$$

where E_1 and μ_1 represent the deformation modulus and Poisson's ratio in the horizontal plane, E_2 and μ_2 are vertical deformation modulus and Poisson's ratio, G_2 represents the tangential modulus of the vertical plane.

With the roller condition applied at the lateral boundaries, the following results are obtained on both the $x=0$ and $x=a$ end planes.

$$u=0\tau_{xz}=0 \tag{18}$$

Similarly on the two end faces of $y=0$ and $y=b$ there are

$$v=0\tau_{yz}=0 \tag{19}$$

When the bottom condition is rough, there is no displacement in all directions on the lateral boundaries. When the bottom conditions are smooth, in the absence of shear stress at the bottom and also without vertical displacement.

With variable separations, the horizontal displacement $u(x,y,z)$ can be expressed as follows

$$u(x,y,z)=\sum_{m=1}^{\infty}\sum_{n=1}^{\infty}f_{mn}^{u}X_m(x)Y_n(y) \tag{20}$$

where $X_m(x)$ and $Y_n(y)$ are all known functions that satisfy the corresponding boundary conditions with f_{mn}^{u} taken as a polynomial (and for simplicity a linear one). Taking both $X_m(x)$ and $Y_n(y)$ in the form of a beam function, the displacement function in each direction can be expressed as follows since the roller condition is used at the boundary.

$$\left.\begin{aligned} u(x,y,z)&=\sum_{m=0}^{\infty}\sum_{n=0}^{\infty}f_{mn}^{u}\sin k_m x\cos k_n y \\ v(x,y,z)&=\sum_{m=0}^{\infty}\sum_{n=0}^{\infty}f_{mn}^{v}\cos k_m x\sin k_n y \\ w(x,y,z)&=\sum_{m=0}^{\infty}\sum_{n=0}^{\infty}f_{mn}^{w}\sin k_m x\sin k_n y \end{aligned}\right\} \tag{21}$$

When the thickness of the layer element is small, f_{mn}^{u}, f_{mn}^{v} and f_{mn}^{w} can be considered to vary linearly, i.e.

$$f_{mn}^{u}=u_{mn}^{i}+\frac{u_{mn}^{i}-u_{mn}^{j}}{c}\cdot z$$

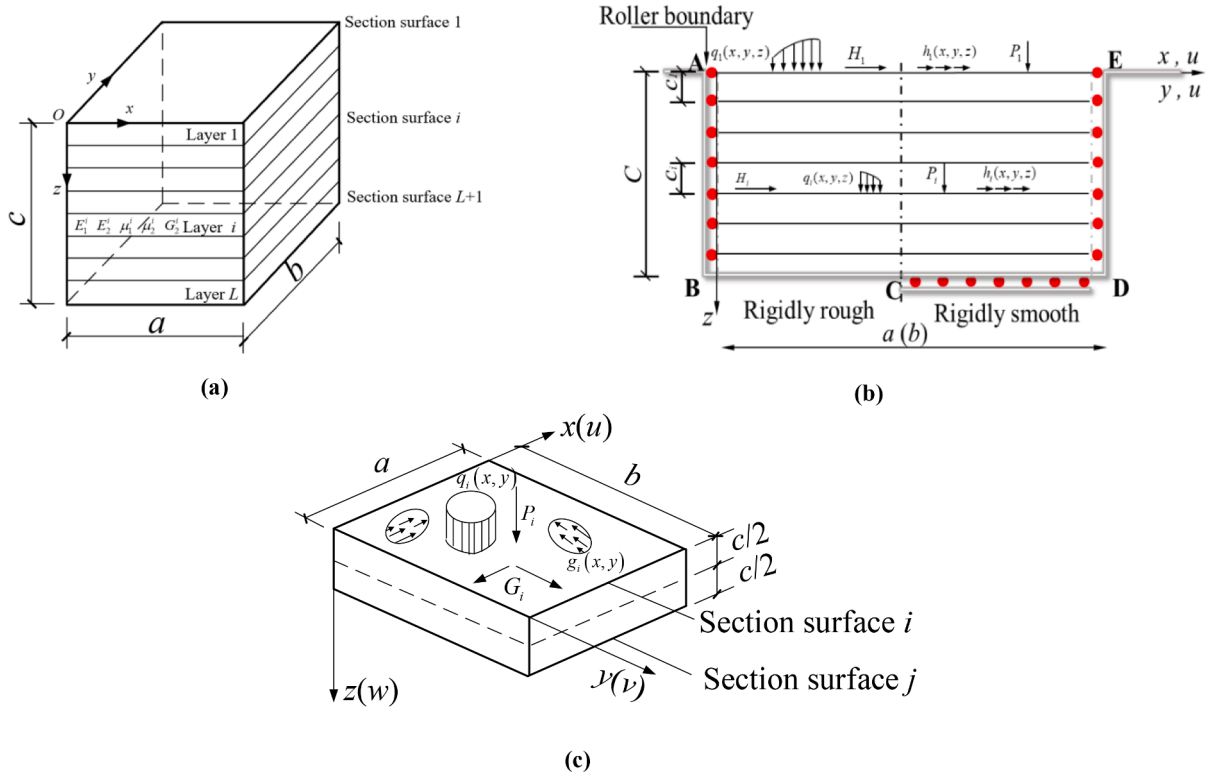

Fig. 3. Schematic diagram of the finite layer model associated with the mechanical field (a) Spatial physical model (b) Boundary conditions and support conditions (c) Typical layer element model.

$$f_{mn}^{v} = v_{mn}^{i} + \frac{v_{mn}^{i} - v_{mn}^{j}}{c} \cdot z$$

$$f_{mn}^{w} = w_{mn}^{i} + \frac{w_{mn}^{i} - w_{mn}^{j}}{c} \cdot z \tag{22}$$

where i and j indicate the upper and lower surfaces and c is the thickness of the layer element. In making the following provisions:

$$\bar{z} = z/c\{\delta\}_{mn} = \left[u_{mn}^{i} \quad v_{mn}^{i} \quad w_{mn}^{i} \quad u_{mn}^{j} \quad v_{mn}^{j} \quad w_{mn}^{j}\right]^{T}\{f\} = [u \quad v \quad w]^{T} \tag{23}$$

Eq. (22) can be rewritten in the following form

$$\{f\} = \sum_{m=0}^{r}\sum_{n=0}^{s}[N]_{mn}\{\delta\}_{mn} \tag{24}$$

where z is the vertical position of the point to be calculated, $\{\delta\}_{mn}$ is the displacement vector of the nodal surface of the displacement layer element and $\{f\}$ is the displacement matrix of displacement layer elements. r and s in Eq.(24) are the number of terms taken in the calculation, $[N]_{mn}$ is the matrix of form functions of the layer elements and can be expressed as

$$[N]_{mn} = \begin{bmatrix} (1-\bar{z})\sin k_m x\cos k_n y & 0 & 0 \\ 0 & (1-\bar{z})\cos k_m x\sin k_n y & 0 \\ 0 & 0 & (1-\bar{z})\cos k_m x\cos k_n y \\ \bar{z}\sin k_m x\cos k_n y & 0 & 0 \\ 0 & \bar{z}\cos k_m x\sin k_n y & 0 \\ 0 & 0 & \bar{z}\cos k_m x\cos k_n y \end{bmatrix} \tag{25}$$

Based on the energy principle and with the orthogonality of the basis function system, the stiffness matrix of the layer elements is obtained as follows

$$[K]_{mnmn}^{i} = \begin{bmatrix} s_1 & & & & & \\ s_2 & s_3 & & & & \\ s_4 & s_5 & s_6 & & & \\ s_7 & s_8 & s_9 & s_{10} & & \\ s_{11} & s_{12} & s_{13} & s_{14} & s_{15} & \\ s_{16} & s_{17} & s_{18} & s_{19} & s_{20} & s_{21} \end{bmatrix} \tag{26}$$

where $[K]_{mnmn}^{i}$ represents the mnth term stiffness matrix of the layer element I and $s_1 \ldots s_{21}$ are matrix coefficients, which have a specific expansion form in Appendix A. In order to ensure the completeness of the orthogonal function system, the stiffness matrices of the layer elements for $m = 0$ and $n = 0$ need to be discussed separately, and the detailed results are also given in Appendix A.

While the computational domain is divided into N layer elements in the vertical direction, the overall stiffness matrix can be obtained by assembling the bottom condition and the layer element stiffness matrix. The total stiffness matrix is a square matrix of order 3N + 3 when the bottom support condition is smooth, while the total stiffness matrix is of order 3 N when the support condition is rough, as shown in Fig. 4.

With the body and surface forces acting within the typical layer element, the expression of the equivalent load vector $\{f\}_{mn}$ can be obtained as follows

$$\{F\}_{mn} = \int_{v}[N]_{mn}^{T}\{q\}_{v}\mathrm{d}v + \int_{A_i}[N]_{mn}^{T}\{q\}_{i}\mathrm{d}A + \int_{A_j}[N]_{mn}^{T}\{q\}_{j}\mathrm{d}A \tag{27}$$

where $\{f\}_{mn}$ is the equivalent load vector expressed as

$$\{F\}_{mn} = \int_{A_i}\left[F_{i,mn}^{u}F_{i,mn}^{v}F_{i,mn}^{w}F_{j,mn}^{u}F_{j,mn}^{v}F_{j,mn}^{w}\right]^{T}\mathrm{d}A \tag{28}$$

With $\{q\}_i$ and $\{q\}_j$ denoting the surface forces acting on nodes i and j, respectively.

For the modeling of energy pile with FLM as shown in Fig. 5, when

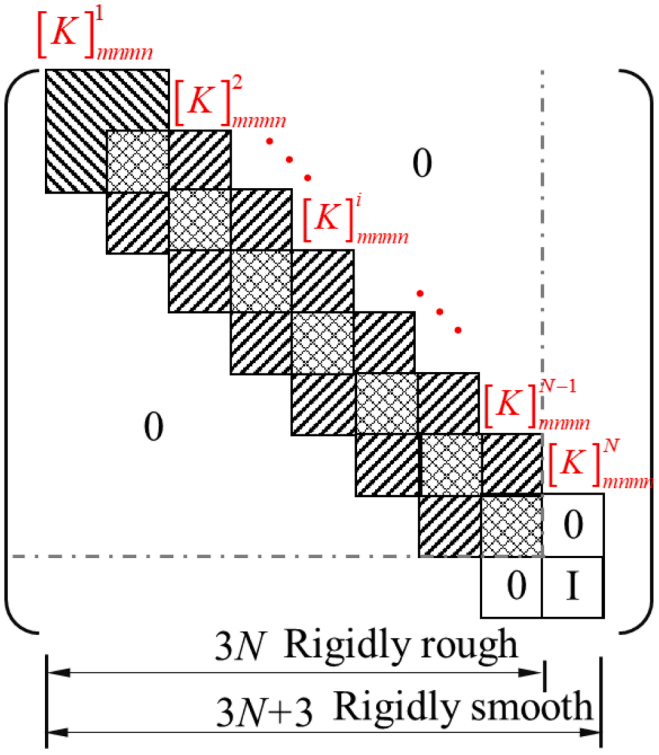

Fig. 4. Assembly schematic of the total stiffness matrix established by the support condition.

consider the vertical force in the z direction, Eq. (28) can be written as

$$\{F\}_{mn} = \int_{A_i} [0\ 0\ \cos k_m x \cos k_n y q(x,y)\ 000]^T \mathrm{d}A \tag{29}$$

in combining Eq.(25). It can be found that the uniform load is distributed along the perimeter of the pile, so the equivalent load in the z-direction can be obtained by doing line integration along the perimeter of the pile.

$$F^w_{i,mn} = q(x,y)\left\{\begin{array}{l} \frac{2}{k_n}\sin k_n \frac{L+d}{2}\left[\cos k_m \frac{L-d}{2} + \cos k_m \frac{L+d}{2}\right] \\ +\frac{2}{k_m}\sin k_m \frac{L+d}{2}\left[\cos k_n \frac{L-d}{2} + \cos k_n \frac{L+d}{2}\right] \end{array}\right\} \tag{30}$$

The values of the equivalent load vectors for $m = 0$ and $n = 0$ need to be discussed separately to ensure the completeness of the function.

Considering the pile as a one-dimensional rod, then its unit stiffness matrix expression is

$$[k]^e_{\mathrm{PP}} = \frac{EA}{l}\begin{bmatrix} 1 & -1 \\ -1 & 1 \end{bmatrix} \tag{31}$$

where $[k]^e_{\mathrm{PP}}$ is unit stiffness matrix of pile, l is the length of the pile unit, E is the deformation modulus of the pile unit, and A is the cross-sectional area of the pile. Assembling the pile unit stiffness matrix into the total stiffness matrix of the pile ($[K]_{\mathrm{pp}}$). The deformation flexibility matrix ($\sum_{m=1}^{r}\sum_{n=1}^{s}[\delta]^{\mathrm{PS}}_{mn}$) of the lateral soil after the pile is stressed can be obtained, so the total stiffness matrix of the joint action of the pile and soil can be expressed as

$$[K] = [K]_{\mathrm{PP}} + [K]_{\mathrm{PS}} = \sum [k]^e_{\mathrm{PP}} + \sum_{m=1}^{r}\sum_{n=1}^{s}[\delta]^{\mathrm{PS}}_{mn}{}^{-1} \tag{32}$$

where $[K]$ is the total stiffness matrix of the joint action of pile and soil and $[K]_{\mathrm{PS}}$ is the total matrix of the stiffness of the deformation of the soil on the side of the pile after the force. By solving the following equations, we can obtain the deformation value of each joint surface after the pile is subjected to the force, and bring it into Eq. (34) to find the magnitude of the lateral resistance to each joint surface.

$$[K]\{\delta\} = \{F\} \tag{33}$$

$$[K]_{\mathrm{PS}}\{\delta\} = \{f\} \tag{34}$$

Where $\{\delta\}$ is a vector of displacement values of each nodal surface, $\{F\}$ is the vector of external load and $\{f\}$ is the vector of lateral resistance to each nodal surface.

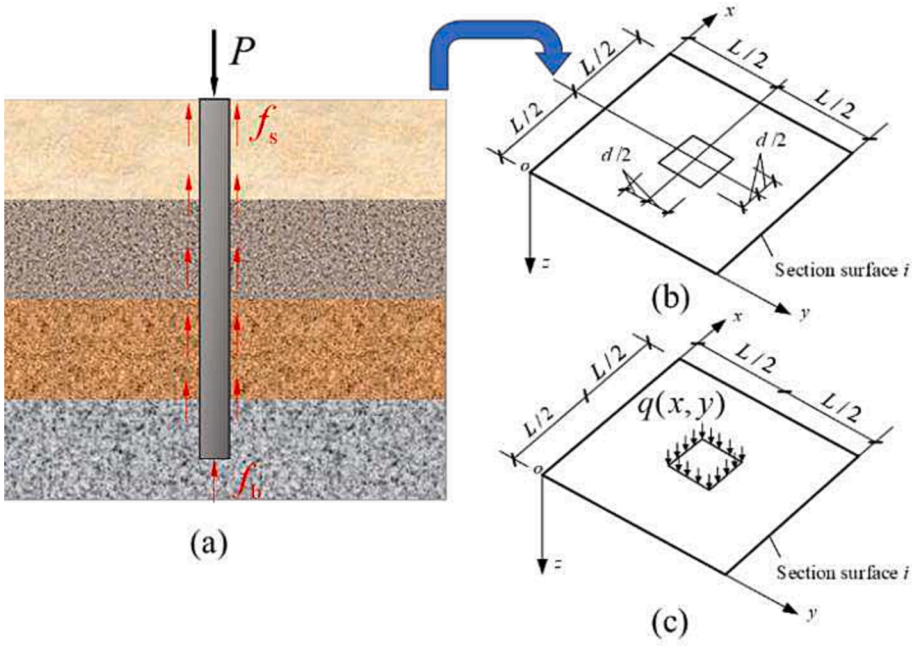

Fig. 5. (a) Schematic diagram of pile-soil synergy (b) Schematic diagram of pile-soil synergy (c) Schematic diagram of the force at section surface.

2.3. Coupled thermo-mechanical analysis for energy piles

Fig. 6 shows the constraint states of energy piles. When the energy pile is not restrained at all, there will be no additional thermal stresses (Fig. 6(a)). Otherwise, when the energy pile is fully restrained, there will be no additional thermal deformation (Fig. 6(b)). In the real state between these two extreme ones, the force balance equation of the energy pile can be written as

$$\left[[K]_{PP} + [K]_{PS}\right]\left\{\{w\}_P + \{w\}_T\right\} = \{F\} + EA\alpha\{d\Delta T\} \tag{35}$$

Where $\{w\}_P$ and $\{w\}_T$ represent the vectors consisting of the displacement values generated by each nodal surface affected by force and temperature, respectively. $\{d\Delta T\}$ is the vector composed by the temperature change of each nodal surface, which is expanded in the following form

$$\{d\Delta T\} = \{-\Delta T_1 \Delta T_1 - \Delta T_2 \cdots \Delta T_i - \Delta T_{i+1} \cdots \Delta T_n\}^T \tag{36}$$

The displacement results at each node of the energy pile under thermal coupling can be obtained by solving Eq. (35). It is then brought into Eq. (34) to obtain the results of the distribution of the lateral resistance along the pile body.

3. Model calibration

3.1. Model Calibration for Soil Temperature Field

3.1.1. Case 0: Effects of the calculation terms M and N in the finite layer analysis method

In the finite layer analysis method for temperature field analysis, increasing the calculation terms M and N in Eq. (5) can theoretically enhance the accuracy of results via a closer approximation to the convergent value. However, it is still imperative to investigate the influence of these terms on the outcomes, since larger amount of terms results in requirement of more computational resources and it may be better to achieve a type of equilibrium with least terms (smallest M and N).

In order to explore the impact of varying values of M and N on temperature calculations at different points within the site, we establish a finite layer model of a homogeneous soil layer with a thermal intensity of 40 W/m. The relevant thermophysical parameters of the soil body are meticulously selected based on previous research and evaluation studies on urban shallow geothermal energy resources, as disclosed in Table 1.

The temperature variations are calculated in an energy pile after three days of operation, with the values of M and N (measured at 0.1 m from the center of the pile) in sites with widths of 10, 20, and 50 m. A schematic diagram was presented in Fig. 7, and the obtained results were illustrated in Fig. 8.

The analysis indicate that temperature changes follow a fluctuating convergence pattern with increasing M and N values. Additionally, the response of temperature changes to M and N alterations varies with different site widths. The smaller the site width, the shorter the period and slower the convergence rate of temperature changes. Conversely, the larger the site width, the longer the period and faster the convergence rate of temperature changes.

Table 1
Calculation parameters table.

Thermal and physical parameters:	value
Thermal conductivity, λ (W/(m K))	2.055
Specific thermal capacity, c (J/(kg K))	854
Density, ρ (kg/m^3)	1959
Thermal intensity, q (W/m)	40
Geometric parameters:	
Thickness, h (m)	20
Width, $2a$ (m)	10, 20 or 50
Width, $2b$ (m)	10, 20 or 50
Time parameters:	
Time increments, Δt (d)	0.01
Time factors, θ	0.8

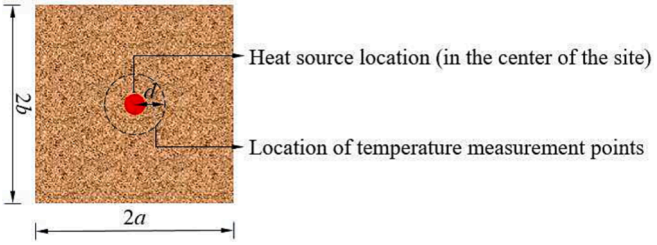

Fig. 7. Location of measurement points and heat sources in the finite layer model.

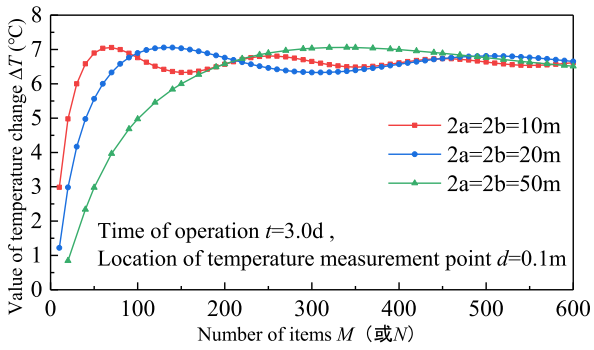

Fig. 8. Curve of temperature change value with M and N.

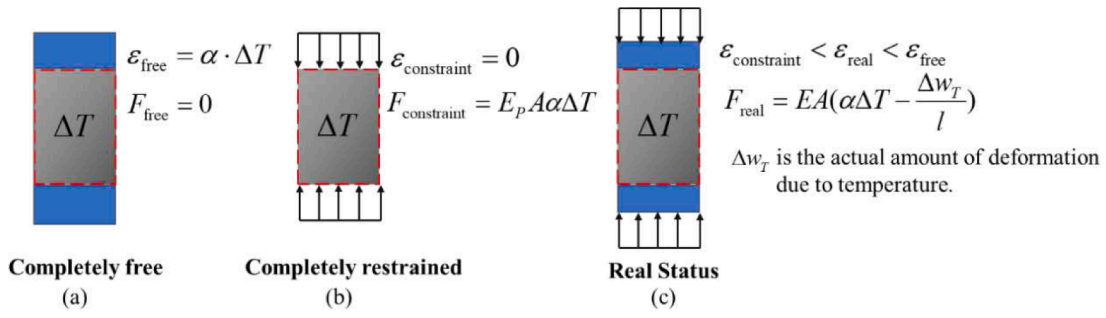

Fig. 6. Schematic diagram of energy piles deformed and stressed by temperature (where ε_{free}, $\varepsilon_{constraint}$ and ε_{real} represent the strains of the energy pile after being subjected to temperature in the completely free, completely confined and real states, respectively. Similarly, F_{free}, $F_{constraint}$, F_{real} represent the additional temperature load of the energy pile after being subjected to temperature in the completely free, completely restrained and real states, respectively. α is the coefficient of thermal expansion of concrete, ΔT is the amount of change in temperature).

To eliminate the calculation errors associated with site size, the study suggests increasing the level term appropriately, as depicted in Fig. 8. Based on the findings, setting M and N values to 500 is recommended in a practical account.

3.1.2. Case 1: Finite long line heat source model by Eskilson (FLS model)

Eskilson and Claesson (1988) introduced the finite long line heat source (FLS) model, which is a modified version of Kelvin's infinite long line heat source model, to better reflect the performance of underground heat exchangers. However, Eskilson did not provide a direct calculation method for determining ground temperature growth under the FLS model. To address this limitation, Zeng et al. (2002), Zeng et al. (2003) conducted an analysis and discussion of the FLS model using the virtual heat source and Green's function method. The resulting equation is shown in Eq. (37), where ρ, z, h are geometric parameters, and their specific meanings can be found in the paper by Zeng et al. (2003); τ is the temperature of any point in semi-infinite space; t is the running time; q is the constant thermal intensity; k and α are the thermal conductivity and thermal diffusivity of the soil, respectively.

In light of the FLS model's potential usefulness, a finite layer soil heat transfer calculation model is established for a homogeneous soil layer with one layer, as illustrated in Fig. 1. The thermal intensity is set to 40 W/m with the site size as 20 m × 20 m. Table 1 shows the thermal physical parameters of the soil used in the model. Using the described methods, the soil temperature distribution around the pile is calculated after 1, 3, 5, and 10 days of energy pile operation, and the comparison results of the two methods are visualized in Fig. 9.

$$\tau = \frac{q}{4k\pi}\int_0^H \left\{ \frac{\operatorname{erfc}\left(\frac{\sqrt{\rho^2+(z-h)^2}}{2\sqrt{\alpha t}}\right)}{\sqrt{\rho^2+(z-h)^2}} - \frac{\operatorname{erfc}\left(\frac{\sqrt{\rho^2+(z+h)^2}}{2\sqrt{\alpha t}}\right)}{\sqrt{\rho^2+(z+h)^2}} \right\} \mathrm{d}h \tag{37}$$

Based on our comparison of the results, it is evident that the finite layer solution and FLS model solution produce similar outcomes. This may lead us to conclude that the finite layer analysis method introduced in this paper accurately describes the heat transfer process of energy piles during extended periods of operation, similar to the FLS model. We can rely on this method to analyze and calculate heat transfer in geotechnical soil surrounding energy piles.

3.1.3. Case 2: Field trial of Southeast University, China

Given that it enables the analysis and solution of temperature fields in stratified soils, the finite layer model has a clear advantage over the FLS model. We present the findings from a long-term in-situ thermal response test of energy piles carried out by Guo et al. (2019) at the Jiulong Lake Campus of Southeast University to further demonstrate the applicability of the finite layer model for heat transfer analysis in stratified soils. Fig. 10 shows the soil's geo-profile and thermal physical parameters. During the test, a variable frequency pump was used to control the water flow rate in the heat exchange tube and an adjustable power heating tube was used to control the thermal intensity. The test was conducted with a constant water flow rate of 0.76 m3/h and a constant heating power of 3 kW from 0 to 72 h. This was followed by a variable heat flow heating mode that used 6 kW from 72 to 96 h, 3 kW from 96 to 144 h, and 6 kW from 144 to 188 h. Although the finite layer model of soil heat transfer is not capable of simulating alternating heating power, we focus only on the lateral temperature change of the pile and the temperature growth of the 1# temperature measurement hole, located 0.5 m from the center of the pile, under the constant flow rate and power from 0 to 72 h.

The actual heating power in the thermal response test is used as the thermal intensity in the finite layer analysis method of soil heat transfer, and the finite layer model shown in Fig. 1 is established. In order to demonstrate its merits and determine its correctness, the results of the finite layer model were compared with the measured results. In addition, a three-dimensional finite element model of the soil temperature field was built using COMSOL to simulate in-situ thermal response testing of energy piles. Fig. 11 depicts the model which has a 20 m × 20 m × 30 m size. In this model, the energy pile is simplified to a 1D linear heat source, and the soil parameters are kept consistent with those presented in Fig. 10. In the COMSOL model, the lateral boundaries of the soil are set as constant temperature boundaries and the upper and lower boundaries are set as adiabatic boundaries. The initial temperature of the soil is assumed to be uniform along the depth.

The temperature variation of the 1# temperature measurement hole at various depths over a period of 72 h is calculated using the COMSOL model and finite layer model. The results are then compared to the measured values. Fig. 12 displays the comparison of each model with the field experimental results. The findings indicate that both the finite layer model and the COMSOL model share similar results and accurately reflect the measured results. Nevertheless, some disparities persist between the models and the measured results, specifically at the 72 h of energy pile operation. We subsequently examine the possible reasons for this finding and attribute it to the fact that the heating power is increased to 6 kW after 72 h of operation in the field test. The differences at other time points could, however, be as a result of the complex

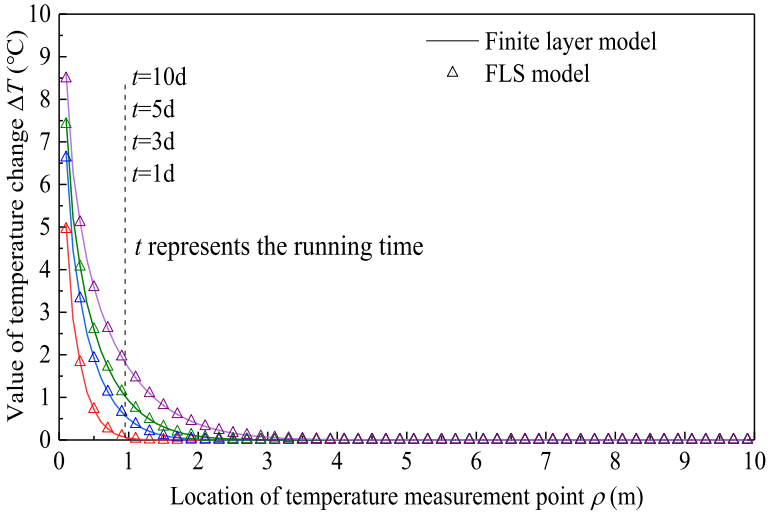

Fig. 9. Comparison of calculation results between finite layer model and FLS model.

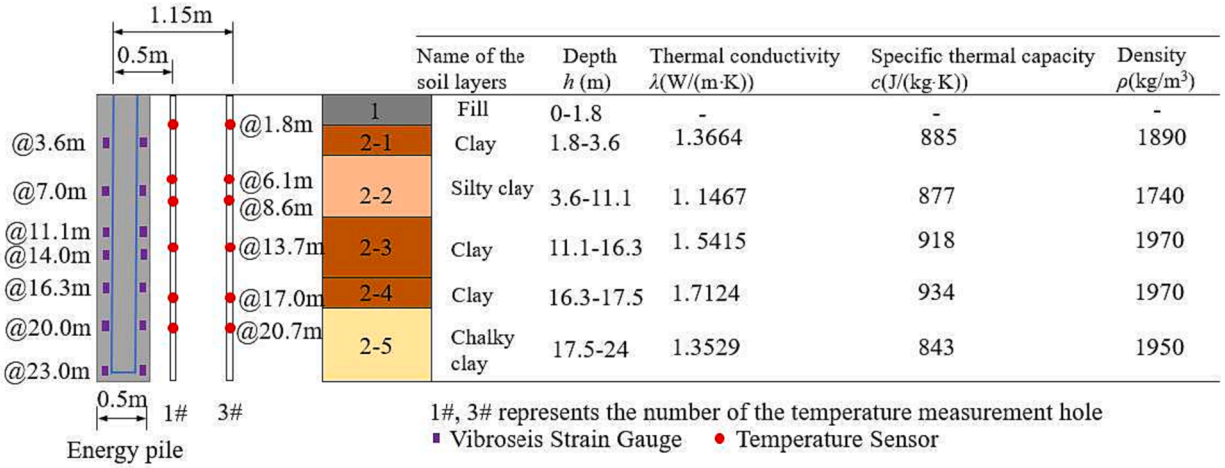

Name of the soil layers	Depth h (m)	Thermal conductivity λ(W/(m·K))	Specific thermal capacity c(J/(kg·K))	Density ρ(kg/m^3)
1 Fill	0-1.8	-	-	-
2-1 Clay	1.8-3.6	1.3664	885	1890
2-2 Silty clay	3.6-11.1	1. 1467	877	1740
2-3 Clay	11.1-16.3	1. 5415	918	1970
2-4 Clay	16.3-17.5	1.7124	934	1970
2-5 Chalky clay	17.5-24	1.3529	843	1950

Fig. 10. Geo-profile and thermal physical parameters of soils for the testing at Southeast University.

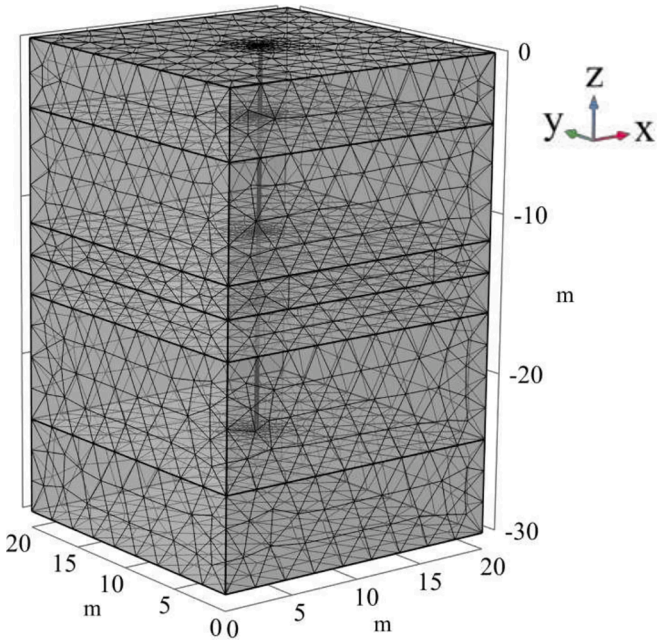

Fig. 11. Finite element model built by COMSOL.

geological conditions and the selection of thermal property parameters of the soil. In general, both models accurately capture the temperature fluctuations in soil due to energy pile operations. The calculations prove the correctness of the COMSOL model and validate the applicability of the finite layer model in solving the temperature field associated with the deformed soil. When comparing the two models, the finite layer model has a significant advantage since it can enhance computational accuracy by merely controlling the expansion term of the level, making it more efficient than the COMSOL model, which is in nature an FEM model.

In addition, the values of the lateral temperature variation along the depth of the pile during the operation of the energy pile, from 0 to 72 h, were extracted. The values obtained were compared with those of the finite layer model and the COMSOL model, and these values were in turn compared with the measured results, as shown in Fig. 13. The heating power is set to 6 kW during the 72-hour test, resulting in slightly larger values than those calculated by the models. However, better agreement between the measured results and the model calculations is observed for the 24- and 48-hour operation periods. This study demonstrates the applicability of the finite layer model for studying temperature field problems in stratified soils.

Compared to the finite element model established with COMSOL, the finite layer model used in this study offers a more efficient and accurate solution. This is achieved by expressing the temperature distribution in the horizontal plane as a function term level that satisfies the imposed boundary conditions in separating variables. The temperature in the depth direction is expressed in a one-dimensional linear discrete manner, thus converting the three-dimensional geotechnical heat conduction problem into a two-dimensional one, which greatly improves the calculation efficiency and accuracy, and yields results that meet engineering requirements.

3.2. Model calibration for thermo-mechanical coupling

3.2.1. Case 3: Field trial of Lambeth College, London, UK

The energy pile tests conducted at Lambeth College premises in South London are widely utilized as a standard benchmark for the validation and calibration of a plethora of energy pile numerical models, both analytical and non-analytical in nature. The pile's geometric configuration is depicted in Fig. 14 along with the ground profile assessment based solely on the results of the standard penetration test (SPT). Further insights into the field set-up, instrumentation, and test elements layout are available in Bourne-Webb et al. (2009). The test involved two piles - the primary testing pile and the heat sink pile. With a mechanical load of 1200kN imposed on the primary testing pile, the pile's head was permitted to move while a load cell regulated the mechanical load. The pile was subjected to cooling for 31 days under the mechanical load, followed by heating for 12 days. The pile was then cycled through daily cycles of heating and cooling for three days. The thermal load administered to the heat sink pile was the inverse of that administered to the primary testing pile. It is noteworthy that the magnitude of the applied thermal load was considerably higher than that utilized in conventional GSHP operations.

Utilizing the finite layer analysis method and based on the parameters provided in Fig. 14, the distribution of axial force and lateral friction resistance of the pile are calculated following its reloading to 1200kN, under conditions of coupled cooling and heating. The ensuing comparison between the calculated outcomes and experimental measurements are illustrated in Fig. 15.Fig. 16

The results generated by the FLM model accurately reflect the field measurements, as evidenced by the lateral friction resistance distribution curve in Fig. 15(b), which highlights the neutral surface of the energy pile's thermal effect at approximately 8.5 m. This further confirms the robustness of the methodology established in this paper.

Prior to temperature fluctuations, the lateral frictional force resulting

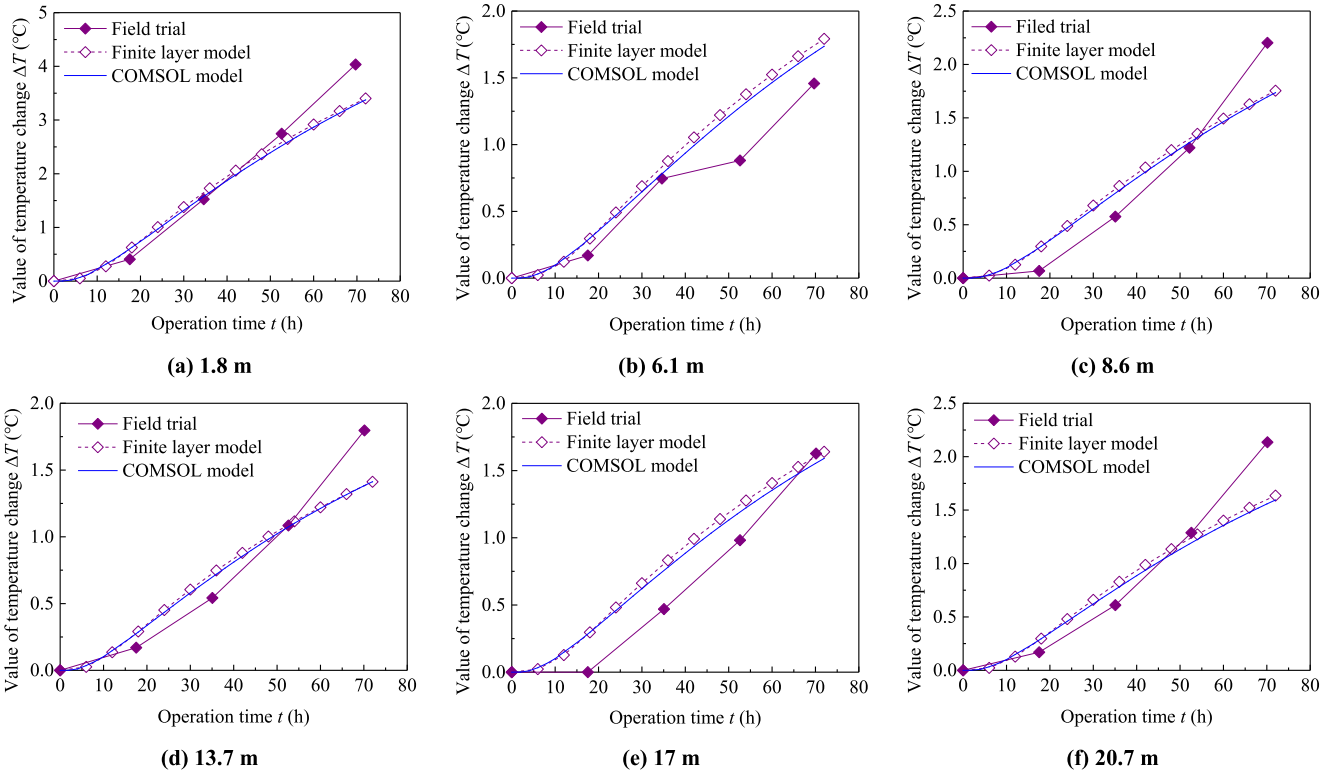

Fig. 12. Temperature increasing curve at different depth in the 1# temperature measurement hole.

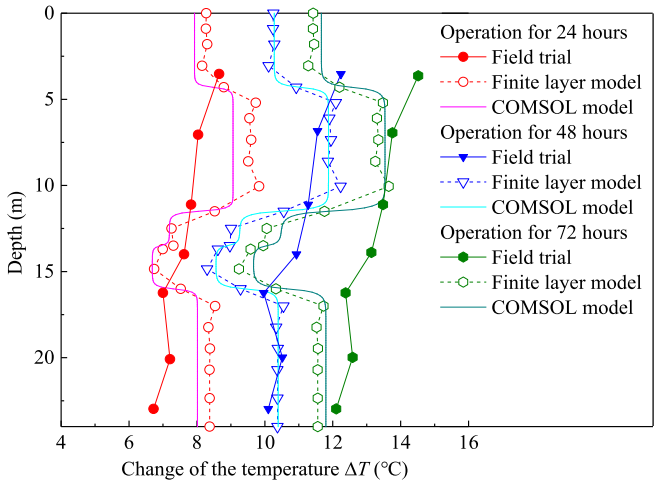

Fig. 13. Temperature variation along depth.

from the loading experiences negligible variation along the depth direction, remaining approximately uniform at an average value of 30 kPa. However, when the energy pile is in use and subjected to heating, the axial force along the depth of the pile increases in all directions, occasioning decreases in the lateral frictional resistance above the neutral point and augmentations below it, triggered by the thermal expansion of the pile. The FLM model aptly captures this phenomenon, The FLM captures this phenomenon well and, as shown in Fig. 15(a), there is no denying that the results of the back analysis model built by Yi & Soga (2011) do work better than the FLM. However, it is worth noting that the results of the initial model developed by Yi & Soga (2011) are far inferior to those of the FLM. The back analytical model is calculated as a correction of the soil stiffness parameters at different temperatures based on the available test data, so the results are naturally better than the FLM. But the soil stiffness parameters used in this model are not actual stiffnesses. In summary, affirming the viability of the coupled thermal- mechanical finite layer analysis method in characterizing and examining load transfer during energy pile operation.

In cooling operation, the effect on the vertical stress and shaft resistance is opposite to that of heating. The pile contracts, resulting in a reduction of its shaft resistance relative to the load-only condition, while shaft resistance above the neutral point increases and decreases below it. It is important to note that cooling generates tensile force at the pile end, necessitating that energy pile design accommodates for this. From the comparison between FLM model outcomes and field tests, it is evident that the finite layer analysis method applies suitably to energy pile cooling conditions as well.

3.2.2. *Case 4: Field trial of EPFL, Lausanne, Switzerland*

The field trial carried out in Lausanne was conducted at Ecole Polytechnique Fédérale de Lausanne (EPFL), Switzerland as part of the construction of a new building on the campus. Fig. 17 provides a brief description of the soil profile, groundwater level, and pile dimensions. For more detailed information, please refer to Laloui et al. (2006). The test pile was employed as a load-bearing and heat-exchanging element throughout the trial. The study comprised seven processes, and in this study, two sets of experiments are selected for the pile top-free condition (Test 1) and after the completion of building construction (Test 7), with the trial results being compared with those obtained from the FLM model. In the case of Test 1, the pile top is free, and no load is being applied, resulting in the energy pile undergoing a heating-recovery process. The comparison results concerning the test and the calculation of the pile top settlement in this particular process are depicted in Fig. 18(a).

Fig. 18(a) depicts the temperature alterations occurring within the energy pile during operation while Fig. 18(b) records the corresponding settlement variations observed at the top of the pile. By deploying the finite layer model, we compute the pile-top settlement throughout the temperature change and contrast our outputs with the empirical results

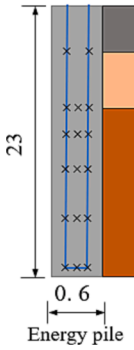

Name of the soil layers	Depth h (m)	Thermal conductivity λ(W/(m·K))	Specific thermal capacity c(J/(kg·K))	Density ρ(kg/m^3)	Modulus Es (Mpa)	Poisson's ratio μ
Made ground	0-1.5	1.4	950	1800	10	0.2
Terrace deposits	1.5-4	1.4	950	2000	13	0.2
London clay	4-23	1.79	910	2000	70	0.236

Fig. 14. Geo-profile and thermal physical parameters of soils for the testing in Lambeth College, London.

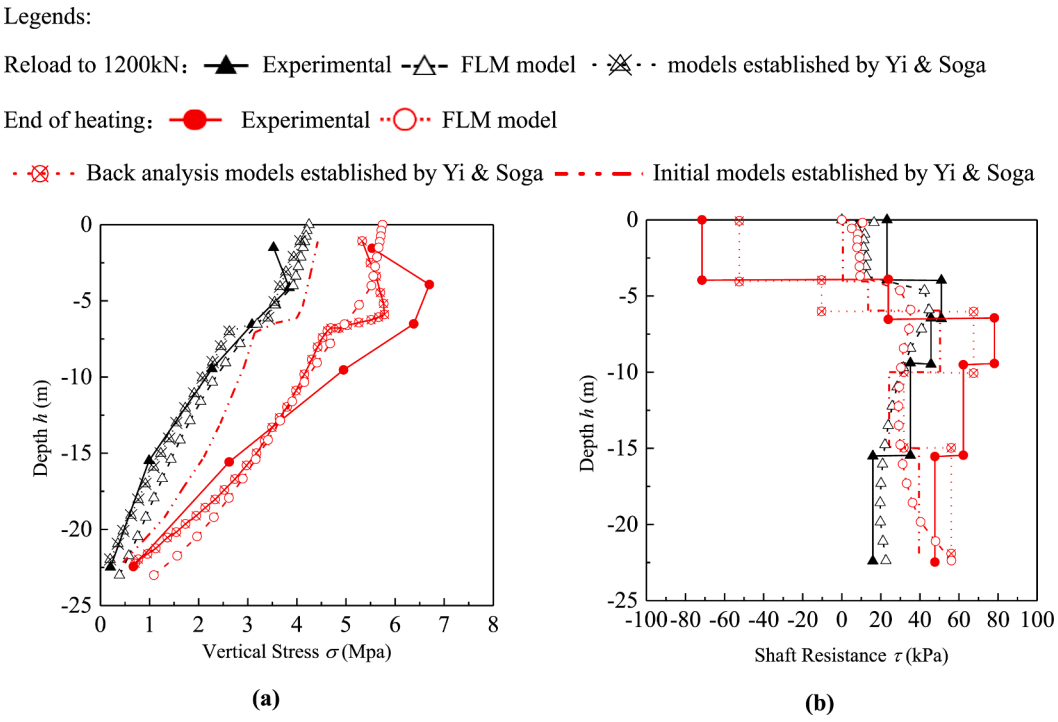

Fig. 15. Comparisons of the vertical stress and shaft resistance measured in different conditions along the length of the test pile between the numerical results and the field data with (a) reload to 1200 kN; (b) combination of the mechanical load and heating by 10 °C.

and finite element calculation results illustrated in Fig. 18(b). We ascertain that the pile-top settlement is contingent upon temperature fluctuations: heating triggers conspicuous bulges atop the pile while cooling brings about settlement. Since temperature discrepancies can cause soil deformation, and as the pile temperature after the heating test is still 3 °C higher than the initial temperature, there will be a certain degree of bulging at the top of the pile at the end of the test. Comparison of the computed results obtained via the finite layer model with the experimental data reveals that the model captures with precision the pile-top displacement in response to temperature variations.

In Fig. 18(c), we present the comparison between the calculated (FLM model and FE model established by Laloui et al. (2006)) and measured thermal strains of piles in the wake of temperature alterations. The non-uniformity of the strain distribution along the pile-body confirms the soil's compressing effect on the pile. Given that the top of the pile is unrestricted in Test 1, soil has a minimal tightening effect on it. When the temperature shift occurred at 21 °C, the measured and calculated thermal strains at the top are 1.93 × 10–4 and 2.09 × 10–4, respectively. With the free pile top, the theoretical value of the thermal strain amounts to 2.1 × 10–4 on this occasion, further validating the correct reflection of the soil's wringing effect on the pile by the finite layer model. Even after cooling down, the energy pile still exhibits a slight thermal strain because the pile-body temperature remains 3 °C higher than the initial temperature. Comprehensively, the results portrayed in Fig. 18 reinforce the applicability of the finite layer model in resolving the thermo-mechanical complexity inherent in energy piles.

In Test 7, the mechanical load placed on the pile-top weighs in at 1088kN, whereas the temperature of the pile rose by 15 °C. By deploying the finite layer model, we simulate the working conditions of Test 7 and compare the findings with the empirical observations, which reveal the model's aptitude for analyzing the stress alterations of piles triggered by thermal and mechanical loading. To further verify the applicability of the FLM, the calculated results were compared with those of the finite element model developed by Laloui et al. (2006), as shown in Fig. 19(b). By comparing the calculated results, it is easy to see that both the finite element model (FE model) and the finite layer model give a good

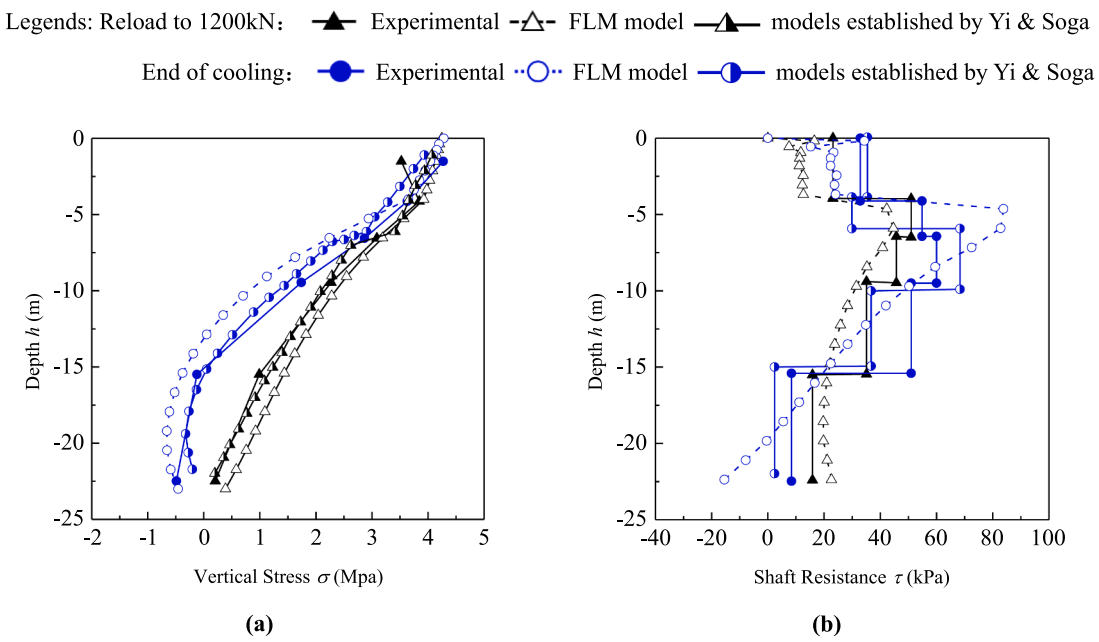

Fig. 16. Comparisons of the vertical stress and shaft resistance measured in different conditions along the length of the test pile between the numerical results and the field data with (a) reload to 1200 kN; (b) combination of the mechanical load and cooling by −19 °C.

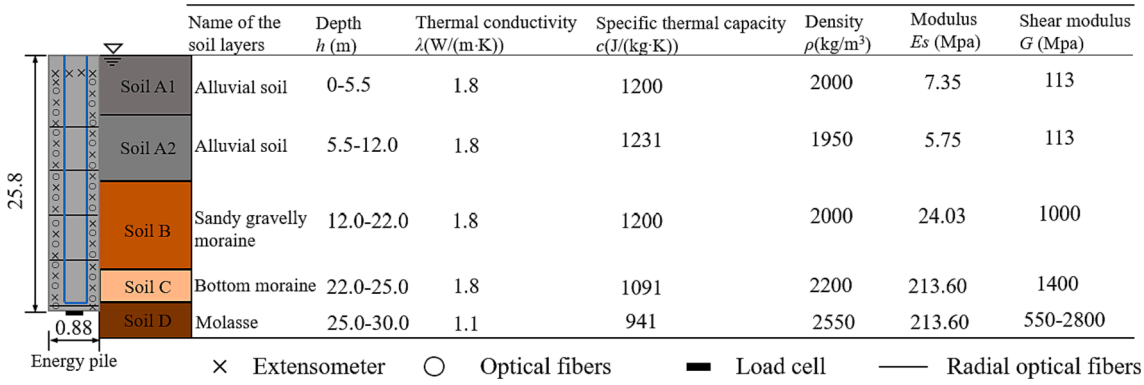

Name of the soil layers	Depth h (m)	Thermal conductivity λ(W/(m·K))	Specific thermal capacity c(J/(kg·K))	Density ρ(kg/m^3)	Modulus Es (Mpa)	Shear modulus G (Mpa)
Alluvial soil	0-5.5	1.8	1200	2000	7.35	113
Alluvial soil	5.5-12.0	1.8	1231	1950	5.75	113
Sandy gravelly moraine	12.0-22.0	1.8	1200	2000	24.03	1000
Bottom moraine	22.0-25.0	1.8	1091	2200	213.60	1400
Molasse	25.0-30.0	1.1	941	2550	213.60	550-2800

Fig. 17. Geo-profile and thermal physical parameters of soils for the testing in EPFL, Lausanne.

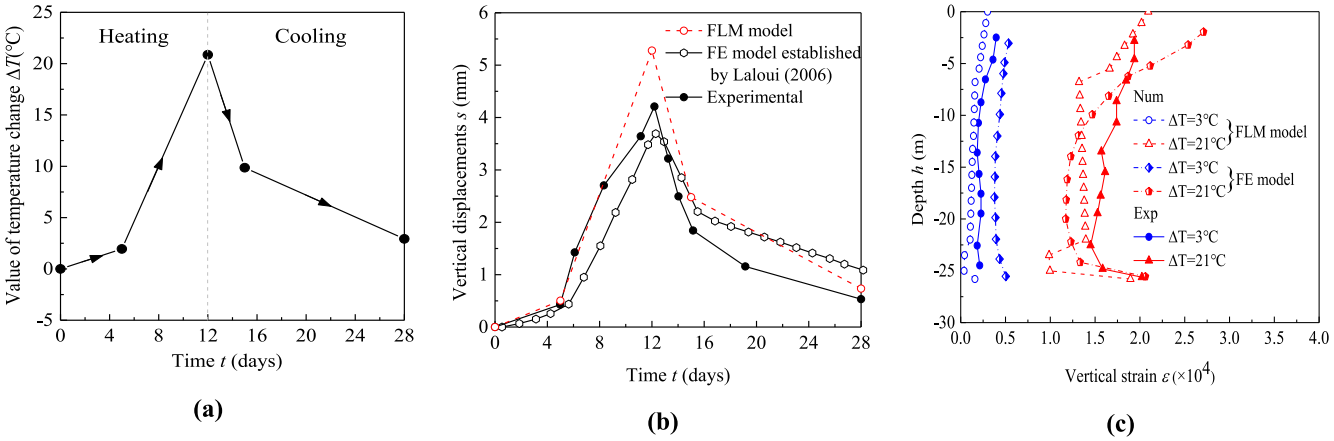

Fig. 18. Comparison of experimental results and calculation results in the Test 1 (a) Value of temperature change in the pile (b) Vertical displacement at pile top (c) Vertical strain of pile shaft.

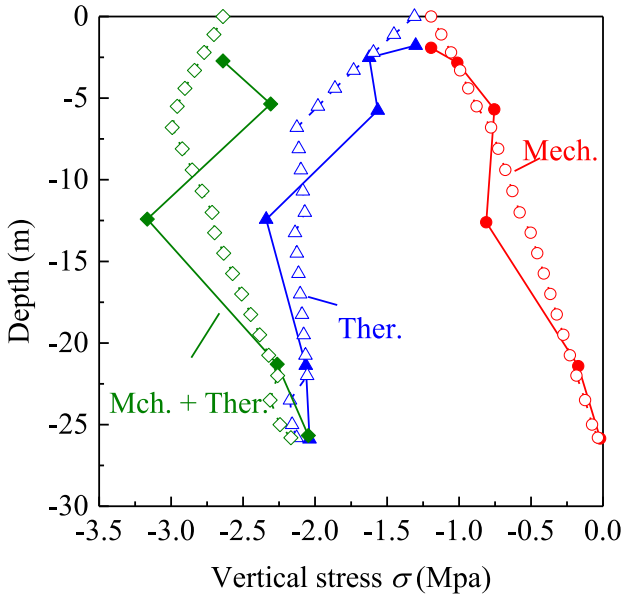

(a)

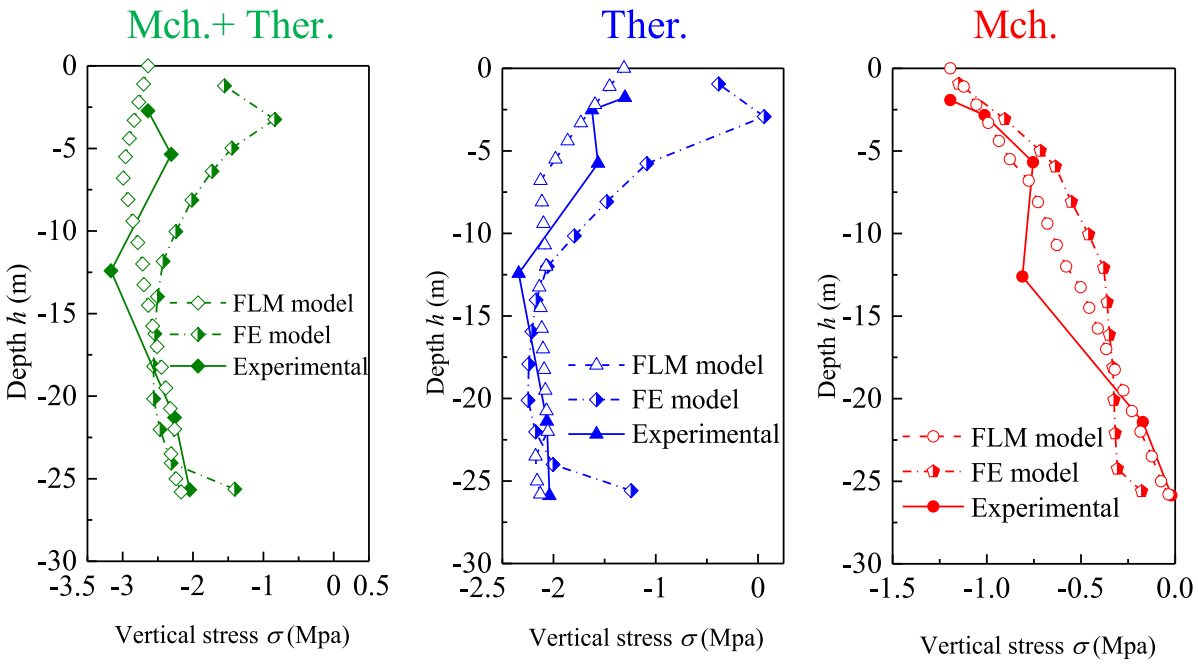

(b)

Fig. 19. Thermo-mechanical vertical stresses in the pile (Test 7) (The hollow points are numerical results, while the solid points are experimental results.)

representation of the distribution of stresses along the pile when only forces are calculated. When coupled thermal-force effects are involved, the results of the finite layer model have better applicability, especially for the upper part of the pile. Tests 1 and 7 yield reliable results when individually subjected to finite layer model analysis, showing the model's promising potential for scrutinizing the effects of thermal and mechanical loading as well as coupled thermo-mechanical impacts on energy piles.

4. Conclusion

In this work, a novel hybrid analytical–numerical method has been put forth on the basis of Finite Layer Analysis Method (FLM) for analyzing the responses of energy piles under thermo-mechanical loads. Suitable for multilayer mediums like soil, FLM reduces a highly complex three-dimensional geotechnical problem to a simplified two-dimensional one, thereby resulting in enhanced computational efficiency in comparison to other methods such as Finite Element Method (FEM).

Consisted of temperature field calculation and thermo-mechanical coupling calculation, the FLM for energy pile has been elaborated before validations against modeling results of other theoretical and numerical methods and field trial data. The FLM results are found to be consistent with those obtained from FEM modeling, but can be

performed with a far better efficiency. The comparisons with the field data of two famous tests (London and Lausanne tests) in the domain of energy pile and with those carried out in Southeast University of China further confirm the accuracy and robustness of the newly proposed FLM method.

CRediT authorship contribution statement

Zong Chenfeng: Conceptualization, Methodology, Formal analysis, Software, Investigation, Writing – original draft. **Jiang Gang:** Conceptualization, Formal analysis, Supervision, Writing – review & editing, Funding acquisition. **Shao Dong:** Methodology, Formal analysis, Investigation, Writing – review & editing. **Wang Xudong:** Supervision, Methodology, Funding acquisition. **Hu Wenbin:** .

Declaration of Competing Interest

The authors declare that they have no known competing financial interests or personal relationships that could have appeared to influence the work reported in this paper.

Data availability

Data will be made available on request.

Acknowledgments

The authors acknowledge financial support provided by The National Natural Science Foundation of China (Grant No. 52201325), The Natural Science Foundation of the Jiangsu Higher Education Institutions of China (Grant No. 21KJB560010), The Foundation of Xuzhou Science and Technology Bureau (Grant No. KC22309 and KC21284), State Key Laboratory of Hydraulic Engineering Simulation and Safety of Tianjin University (Grant No. HESS-2225) and Water Conservancy Science and Technology Project of Jiangsu Province (Grant No. 2020045) from Water Resources Department of Jiangsu Province, China. The computational resources generously provided by the High Performance Computing Center of Nanjing Tech University are greatly appreciated.

Appendix A

The detailed expression and derivation process of each matrix coefficient in the layer element stiffness matrix $[K]^i_{mnmn}$ shown in Eq. (26) is given by finding the derivative of the form function as shown in Eq. (25), which is listed below.

$$[B]_{mn} = [\partial][N]_{mn} = \begin{bmatrix} (1-\bar{z})k_m\cos k_m x\cos k_n y & 0 & 0 & \bar{z}k_m\cos k_m x\cos k_n y & 0 & 0 \\ 0 & (1-\bar{z})k_n\cos k_m x\cos k_n y & 0 & 0 & \bar{z}k_n\cos k_m x\cos k_n y & 0 \\ 0 & 0 & -\dfrac{\cos k_m x\cos k_n y}{c} & 0 & 0 & \dfrac{\cos k_m x\cos k_n y}{c} \\ -(1-\bar{z})k_n\sin k_m x\sin k_n y & -(1-\bar{z})k_m\sin k_m x\sin k_n y & 0 & -\bar{z}k_n\sin k_m x\sin k_n y & -\bar{z}k_m\sin k_m x\sin k_n y & 0 \\ 0 & -\dfrac{\cos k_m x\sin k_n y}{c} & -(1-\bar{z})k_n\cos k_m x\sin k_n y & 0 & \dfrac{\cos k_m x\sin k_n y}{c} & -\bar{z}k_n\cos k_m x\sin k_n y \\ -\dfrac{\sin k_m x\cos k_n y}{c} & 0 & -(1-\bar{z})k_m\sin k_m x\cos k_n y & \dfrac{\sin k_m x\cos k_n y}{c} & 0 & -\bar{z}k_m\sin k_m x\cos k_n y \end{bmatrix} \quad (A.1)$$

By multiplying the above strain matrix with Eq. (17), the elastic matrix in the text gives the stress matrix shown below.

$$[S]_{mn} = [D][B]_{mn}$$

$$= \begin{bmatrix} (1-\bar{z})k_m d_1\cos k_m x\cos k_n y & (1-\bar{z})k_n d_2\cos k_m x\cos k_n y & -\dfrac{d_3\cos k_m x\cos k_n y}{c} & \bar{z}k_m d_1\cos k_m x\cos k_n y & \bar{z}k_n d_2\cos k_m x\cos k_n y & \dfrac{d_3\cos k_m x\cos k_n y}{c} \\ (1-\bar{z})k_m d_2\cos k_m x\cos k_n y & (1-\bar{z})k_n d_1\cos k_m x\cos k_n y & -\dfrac{d_3\cos k_m x\cos k_n y}{c} & \bar{z}k_m d_2\cos k_m x\cos k_n y & \bar{z}k_n d_1\cos k_m x\cos k_n y & \dfrac{d_3\cos k_m x\cos k_n y}{c} \\ (1-\bar{z})k_m d_3\cos k_m x\cos k_n y & (1-\bar{z})k_n d_3\cos k_m x\cos k_n y & -\dfrac{d_4\cos k_m x\cos k_n y}{c} & \bar{z}k_m d_3\cos k_m x\cos k_n y & \bar{z}k_n d_3\cos k_m x\cos k_n y & \dfrac{d_4\cos k_m x\cos k_n y}{c} \\ -(1-\bar{z})k_n d_5\sin k_m x\sin k_n y & -(1-\bar{z})k_m d_5\sin k_m x\sin k_n y & 0 & -\bar{z}k_n d_5\sin k_m x\sin k_n y & -\bar{z}k_m d_5\sin k_m x\sin k_n y & 0 \\ 0 & -\dfrac{d_6\cos k_m x\sin k_n y}{c} & -(1-\bar{z})k_n d_6\cos k_m x\sin k_n y & 0 & \dfrac{d_6\cos k_m x\sin k_n y}{c} & -\bar{z}k_n d_6\cos k_m x\sin k_n y \\ -\dfrac{d_6\sin k_m x\cos k_n y}{c} & 0 & -(1-\bar{z})k_m d_6\sin k_m x\cos k_n y & \dfrac{d_6\sin k_m x\cos k_n y}{c} & 0 & -\bar{z}k_m d_6\sin k_m x\cos k_n y \end{bmatrix} \quad (A.2)$$

In consequence, the expression for the calculation of the layer element stiffness matrix $[K]^i_{mnmn}$ can be derived from the principle of minimum potential energy as follows.

$$[K]^i_{mnmn} = \iiint_V [B]^T[D][B]\mathrm{d}x\mathrm{d}y\mathrm{d}z = \begin{bmatrix} s_1 & & & & & \\ s_2 & s_3 & & & & \\ s_4 & s_5 & s_6 & & & \\ s_7 & s_8 & s_9 & s_{10} & & \\ s_{11} & s_{12} & s_{13} & s_{14} & s_{15} & \\ s_{16} & s_{17} & s_{18} & s_{19} & s_{20} & s_{21} \end{bmatrix} \quad (A.3)$$

The coefficients in the matrix are calculated and sorted according to the above procedure. In order to ensure the completeness of the orthogonal function system, the stiffness matrices of the layer elements for $m = 0$ and $n = 0$ need to be discussed separately. When $m = 0$ and $n = 0$, each coefficient in the matrix can be given with the following expressions:

$$S_1 = S_{10} = abc\frac{d_6}{c^2}S_2 = S_8 = S_{11} = S_{14} = 0 \tag{A.4}$$

$$S_3 = S_{15} = abc\frac{d_6}{c^2}S_4 = S_{19} = 0$$

$$S_5 = S_{20} = 0S_6 = S_{21} = abc\frac{d_4}{c^2}$$

$$S_7 = -abc\frac{d_6}{c^2}S_9 = S_{16} = 0$$

$$S_{12} = -abc\frac{d_6}{c^2}S_{17} = S_{13} = 0$$

$$S_{18} = -abc\frac{d_4}{c^2}$$

When $m = 0$ and $n \neq 0$, each coefficient in the matrix can be expressed as follows:

$$S_1 = S_{10} = \frac{abc}{2}\left(\frac{d_5}{3}k_n^2 + \frac{d_6}{c^2}\right)S_2 = S_8 = S_{11} = S_{14} = 0 \tag{A.5}$$

$$S_3 = S_{15} = \frac{abc}{2}\left(\frac{d_1}{3}k_n^2 + \frac{d_6}{c^2}\right)S_4 = S_{19} = 0$$

$$S_5 = -S_{20} = \frac{abc}{2}(-d_3 + d_6)\frac{k_n}{2c}S_6 = S_{21} = \frac{abc}{2}\left(\frac{d_6}{3}k_n^2 + \frac{d_4}{c^2}\right)$$

$$S_7 = \frac{abc}{2}\left(\frac{d_5}{6}k_n^2 - \frac{d_6}{c^2}\right)S_9 = S_{16} = 0$$

$$S_{12} = \frac{abc}{2}\left(\frac{d_1}{6}k_n^2 - \frac{d_6}{c^2}\right)S_{17} = -S_{13} = \frac{abc}{2}(d_3 + d_6)\frac{k_n}{2c}$$

$$S_{18} = \frac{abc}{2}\left(\frac{d_6}{6}k_n^2 - \frac{d_4}{c^2}\right)$$

When $m \neq 0$ and $n = 0$, each coefficient in the matrix has the following form:

$$S_1 = S_{10} = \frac{abc}{2}\left(\frac{d_1}{3}k_m^2 + \frac{d_6}{c^2}\right)S_2 = S_8 = S_{11} = S_{14} = 0 \tag{A.6}$$

$$S_3 = S_{15} = \frac{abc}{2}\left(\frac{d_5}{3}k_m^2 + \frac{d_6}{c^2}\right)S_4 = -S_{19} = \frac{abc}{2}(-d_3 + d_6)\frac{k_m}{2c}$$

$$S_5 = S_{20} = 0S_6 = S_{21} = \frac{abc}{2}\left(\frac{d_6}{3}k_m^2 + \frac{d_4}{c^2}\right)$$

$$S_7 = \frac{abc}{2}\left(\frac{d_1}{6}k_m^2 - \frac{d_6}{c^2}\right)S_{16} = -S_9 = \frac{abc}{2}(d_3 + d_6)\frac{k_m}{2c}$$

$$S_{12} = \frac{abc}{2}\left(\frac{d_5}{6}k_m^2 - \frac{d_6}{c^2}\right)S_{17} = S_{13} = 0$$

$$S_{18} = \frac{abc}{2}\left(\frac{d_6}{6}k_m^2 - \frac{d_4}{c^2}\right)$$

When $m \neq 0$ and $n \neq 0$, the coefficients in the matrix need to be written as:

$$s_1 = s_{10} = \frac{abc}{4}\left(d_1k_m^2/3 + d_5k_n^2/3 + d_6/c^2\right)s_2 = s_{14} = 2s_8 \tag{A.7}$$

$$s_3 = s_{15} = \frac{abc}{4}\left(d_5k_m^2/3 + d_1k_n^2/3 + d_6/c^2\right)s_4 = -s_{19} = \frac{abc}{4}(-d_3 + d_6)k_m \Big/ 2c$$

$$s_5 = -s_{20} = \frac{abc}{4}(-d_3 + d_6)k_n \Big/ 2cs_6 = s_{21} = \frac{abc}{4}\left(d_6k_m^2/3 + d_6k_n^2/3 + d_4/c^2\right)$$

$$s_7 = \frac{abc}{4}\left(d_1k_m^2/6 + d_5k_n^2/6 - d_6/c^2\right)s_8 = s_{11} = \frac{abc}{4}(d_2 + d_5)k_mk_n \Big/ 6$$

$$s_{12} = \frac{abc}{4}\left(d_5k_m^2/6 + d_1k_n^2/6 - d_6/c^2\right)s_{16} = -s_9 = \frac{abc}{4}(d_3 + d_6)k_m \Big/ 2c$$

$$s_{18} = \frac{abc}{4}\left(d_6 k_m^2/6 + d_6 k_n^2/6 - d_4/c^2\right) s_{17} = -s_{13} = \frac{abc}{4}(d_3 + d_6)k_n \Big/ 2c$$

References

Abas, N., Kalair, A., Khan, N., 2015. Review of fossil fuels and future energy technologies. Futures 69, 31–49.

Amatya, B.L., Soga, K., Bourne-webb, P.J., Amis, T., Laloui, L., 2012. Thermo-mechanical behaviour of energy piles. Thermo-mechanical behaviour of energy piles. Géotechnique 62 (6), 503–519.

Armaleh, S., Desai, C.S., 1987. Load-Deformation Response of Axially Loaded Piles. J. Geotech. Engrg. 113 (12), 1483–1500.

Bölük, G., Mert, M., 2014. Fossil & renewable energy consumption, GHGs (greenhouse gases) and economic growth: evidence from a panel of EU (European Union) countries. Energy 74, 439–446. https://doi.org/10.1016/j.energy.2014.07.008.

Booker, J.R., Small, J.C., 1982. Finite layer analysis of consolidation-1. Int. J. Numer. Anal. Meth. Geomech. 6 (2), 151–171. https://doi.org/10.1002/nag.1610060204.

Booker, J.R., Small, J.C., 1984. The time-deflection behavior of a circular raft of finite flexibility on a deep clay layer. Int. J. Numer. Anal. Methods Geomech. 8, 343–357. https://doi.org/10.1002/nag.1610080404.

Booker, J.R., Small, J.C., 1986. Finite layer analysis of viscoelastic layered materials. Int. J. Numer. Anal. Meth. Geomech. 10, 415–430. https://doi.org/10.1002/nag.1610100406.

Bourne-Webb, P.J., Amatya, B., Soga, K., Amis, T., Davidson, C., Payne, P., 2009. Energy pile test at lambeth college, London: Geotechnical and thermodynamic aspects of pile response to heat cycles. Géotechnique 59 (3), 237–248.

Brandl, H., 2006. Energy foundations and other thermo-active ground structures. Géotechnique 56, 81–122. https://doi.org/10.1680/geot.2006.56.2.81.

Castelli, F., Maugeri, M., 2002. Simplified Nonlinear Analysis for Settlement Prediction of Pile Groups. J. Geotech. Geo-environ. Eng. 28, 76–84. https://doi.org/10.1061/(asce)1090-0241(2002)128:1(76).

Chakrabarti, S., 1980. Heat Conduction in Plates by Finite Strip Method. J .Eng. Mech. Div. 106 (2), 233–244.

Cheung, Y.K., 1976. Finite strip method in structural analysis. Pergamon Press.

de Moel, M., Bach, P.M., Bouazza, A., Singh, R.M., Sun, J.O., 2010. Technological advances and applications of geothermal energy pile foundations and their feasibility in Australia. Renew. Sustain. Energy Rev. 14 (9), 2683–2696.

Di Donna, Ai., Laloui, L., 2015. Numerical analysis of the geotechnical behaviour of energy piles. Int. J. Numer. Anal. Methods Geomech. 39, 8, 861–888. https://doi.org/10.1061/10.1002/nag.2341.

Eskilson, P., Claesson, J., 1988. Simulation model for thermally interacting heat extraction boreholes. Numer. Heat Transf. 13 (2), 149. https://doi.org/10.1080/10407798808551378.

Guo Y.M., et al., 2019. Prototype experimental investigation on the thermo-mechanical behaviors of free constrained full-scale PHC energy piles in multi-layer strata. J. Rock Mech. Geotech. Eng. 38, 3, 582–590. https://doi.org/10.13722/j.cnki.jrme.2018.1073.

Knellwolf, C., Peron, H., Laloui, L., 2011. Geotechnical analysis of heat exchanger piles. J. Geotech. Geoenviron. Eng. 137 (10), 890–902.

Kramer C.A., 2013. An experimental investigation on performance of a model geothermal pile in sand, 104.

Laloui, L., Nuth, M., Vulliet, L., 2006. Experimental and numerical investigations of the behaviour of a heat exchanger pile. Int. J. Numer. Anal. Meth. Geomech. 30 (8), 763–781.

Leung, Y.F., et al., 2010. Coupled foundation-superstructure analysis and influence of building stiffness on foundation response. in ASCE Geotechnical Special Publication 205 - Deep Foundations and Geotechnical In-Situ Testing, 61–66. https://doi.org/10.1061/41106(379)6.

Mei G.X, Zai J.M., 2006. Theory and application of consolidation finite layer. Beijing: Sciences Press.

Murphy, K.D., et al., 2013. Behavior of Full-Scale Energy Foundations in Denver, Colorado. Biennial Geotech. Semin. 7, 2017–2229. https://doi.org/10.1061/9780784412633.0015.

Ouyang, Y., et al., 2011. Numerical back-analysis of energy pile test at Lambeth College, London. In: Geo-Frontiers, pp. 440–449. https://doi.org/10.1061/41165(397)46.

Plaseied, N., 2012. Load-transfer analysis of energy foundations. John S. McCartney. University of California San Diego.

Said, I., De Gennaro, V., Frank, R., 2009. Axisymmetric finite element analysis of pile loading tests. Comput. Geotech. 36 (1-2), 6–19.

Small, J.C., Booker, J.R., 1986. Finite layer analysis of layered elastic materials using a flexibility approach. Part 2—Circular and rectangular loadings. Int. J. Numer. Meth. Eng. 23, 959–978. https://doi.org/10.1002/nme.1620230515.

Smith, S.S., Allen, M.B., Puckett, J., Edgar, T., 1992. The finite layer method for groundwater flow models. Water Resour. Res. 28 (6), 1715–1722.

Sørensen, B., 2008. A sustainable energy future: Construction of demand and renewable energy supply scenarios. Int. J. Energy Res., 32, 36–70.

Sugiawan, Y., Managi, S., 2019. New evidence of energy-growth nexus from inclusive wealth. Renew. Sustain. Energy Rev. 103, 40–48. https://doi.org/10.1016/j.rser.2018.12.044.

Suryatriyastuti, M.E., Mroueh, H., Burlon, S., 2014. A load transfer approach for studying the cyclic behavior of thermo-active piles. Comput. Geotech. 55, 378–391. https://doi.org/10.1016/j.compgeo.2013.09.021.

Wang, X.D., et al., 1994. Analysis of pile groups-soil-pile cap interaction by the finite layer method and finite element method. J. Nanjing Arch. Civil Eng. Inst. 30 (3), 1–8.

Wang, X.D., et al., 1996. Numerical analysis of pile group-soil-pile cap interaction. Chin. J. Geotech. Eng. 18 (4), 27–33.

Wang, X.D., et al., 2009. Finite layer method for numerical simulation of unsteady groundwater flow in cylindrical coordinate system. Chin. J. Geotech. Eng. 31 (1), 15–20.

Wang, B., et al., 2012. Field and Laboratory Investigation of a Heat Exchanger Pile. ASCE. 225, 4396–4405. https://doi.org/10.1061/9780784412121.452.

Wang, B., Bouazza, A., Singh, R.M., Haberfield, C., Barry-Macaulay, D., Baycan, S., 2015. Bouazza A, Singh RM, Haberfield C, Barry-Macaulay D, Baycan S. Posttemperature Effects on Shaft Capacity of a Full-Scale Geothermal Energy Pile. J. Geotech. Geoenviron. Eng. 141 (4) https://doi.org/10.1061/(asce)gt.1943-5606.0001266.

Zeng, H., et al., 2002. Analysis on steady-state temperature field around a vertical borehole in geothermal heat exchangers. J. Shandong Inst. Arch. Eng. 17 (1), 1–6.

Zeng, H., Diao, N., Fang, Z., 2003. Fang Z. Heat transfer analysis of boreholes in vertical ground heat exchangers. Int. J. Heat Mass Transf. 46 (23), 4467–4481.